Letters

A Source Stirred Reverberation Chamber Using a Robotic Arm

Qian Xu, *Member, IEEE*, Lei Xing, *Member, IEEE*, Yongjiu Zhao, Tianyuan Jia, and Yi Huang, *Senior Member, IEEE*

***Abstract*—In a reverberation chamber, the stirring efficiency of the source stir technique is very high. However, to apply the source stir, the configuration (position, orientation, or polarization) of the transmitting (Tx) antenna has to be changed every time in the stirring process. To solve this problem, we use a three-dimensional printed robotic arm to control the position and orientation of the Tx antenna; thus, the source stirring process can be performed automatically. The measurement results are validated and compared with that from mechanical stirrers. Figures of merit such as autocorrelation, average *K*-factor, and total scattering cross-section are presented. The statistical distribution is also verified by using Kolmogorov–Smirnov test. Results show that the source stir technique outperforms the mechanical stirring technique significantly.**

***Index Terms*—Electromagnetic compatibility, random media, reverberation chamber.**

I. Introduction

A REVERBERATION chamber (RC) has been widely used in the area of electromagnetic compatibility (EMC) [1]–[3] and over-the-air (OTA) test [4]–[9]. In an RC, random electromagnetic (EM) fields can be generated by many stirring techniques, such as mechanical stir, frequency stir, and source stir.

From a theoretical perspective, to stir the EM field inside a cavity with a high-quality (Q) factor, we need to change the boundary configurations or change the source distribution inside it ($\mathbf{E} = \iiint \overline{\overline{\mathbf{G}}}\mathbf{J}ds'$, change the dyadic Green's function $\overline{\overline{\mathbf{G}}}$ or the source distribution $\mathbf{J}$). The source stir technique has been proposed and investigated in [10]–[23]. If the source is used as a stationary coordinate system, source stir is actually stirring the whole RC [24]. Thus, the source stir technique can have a very high stirring efficiency, which has been experimentally proven in [24]. Another advantage is that the source stir technique does not require large stirrers which occupy large volumes in an RC (the RC itself is a stirrer if the source is used as the stationary coordinate system), and the available test area could be increased significantly.

However, in the previous work, the source is moved manually [24] or switched in sequence [13], very limited antenna positions can be obtained. In this paper, we use a robotic arm to control the position and orientation of a transmitting (Tx) antenna inside an RC which is easy to generate a large number of samples. Results are validated and compared with mechanical stirrers.

The system configurations are given in Section II, measurement results are detailed in Section III where the figures of merit such as autocorrelation, average *K*-factor, and total scattering cross-section are calculated and compared with conventional mechanical stirrers. Section IV summarizes the conclusion.

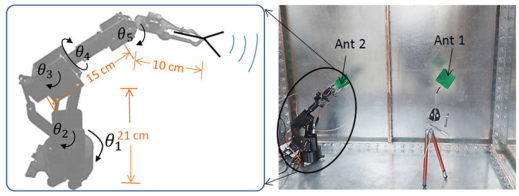

(a) (b)

Fig. 1. Measurement setup in an RC. (a) Robotic arm. (b) Measurement scenario in an RC. Dimensions of the RC are 1.2 m × 1.2 m × 0.8 m.

II. Measurement Setup

The system setup is illustrated in Fig. 1. The lowest usable frequency (LUF) of the RC is about 1 GHz [25]. A robotic arm in Fig. 1(a) is manufactured by applying 3-D printing technology (using polylactic acid), which has 5 degrees of freedom (DoF): θ_i, $i = 1 \ldots 5$. An antenna (Ant 2) is fixed at the end of the robotic arm that can be moved with 5 DoF in space (in a volume of 45 cm × 45 cm × 50 cm). Ant 1 and Ant 2 are wideband dipole antennas which are the same as that used in [26]; they are connected to a vector network analyzer (VNA) through the bulkheads on the wall of the RC. A computer controls the movement of the robotic arm and the trigger of the VNA. For each position of Ant 2, the computer records the measured *S*-parameters. The measurement flowchart is shown in Fig. 2.

Manuscript received March 9, 2019; accepted April 14, 2019. This work was supported in part by the National Natural Science Foundation of China under Grants 61701224 and 61601219, and in part by the Nature Science Foundation of Jiangsu Province under Grant BK20160804. *(Corresponding author: Qian Xu.)*

Q. Xu, L. Xing, and Y. Zhao are with the College of Electronic and Information Engineering, Nanjing University of Aeronautics and Astronautics, Nanjing 211106, China (e-mail: emxu@foxmail.com; emxinglei@foxmail.com; yjzhao@nuaa.edu.cn).

T. Jia and Y. Huang are with the Department of Electrical Engineering and Electronics, The University of Liverpool, Liverpool L69 3GJ, U.K. (e-mail: tianyuan.jia@liv.ac.uk; yi.huang@liverpool.ac.uk).

Color versions of one or more of the figures in this letter are available online at http://ieeexplore.ieee.org.

Digital Object Identifier 10.1109/TEMC.2019.2912999

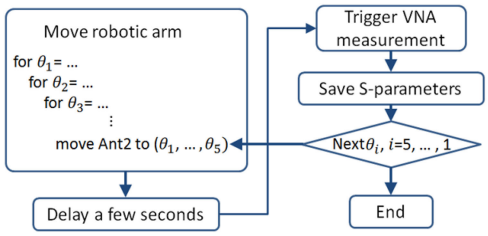

Fig. 2. Flowchart of the measurement.

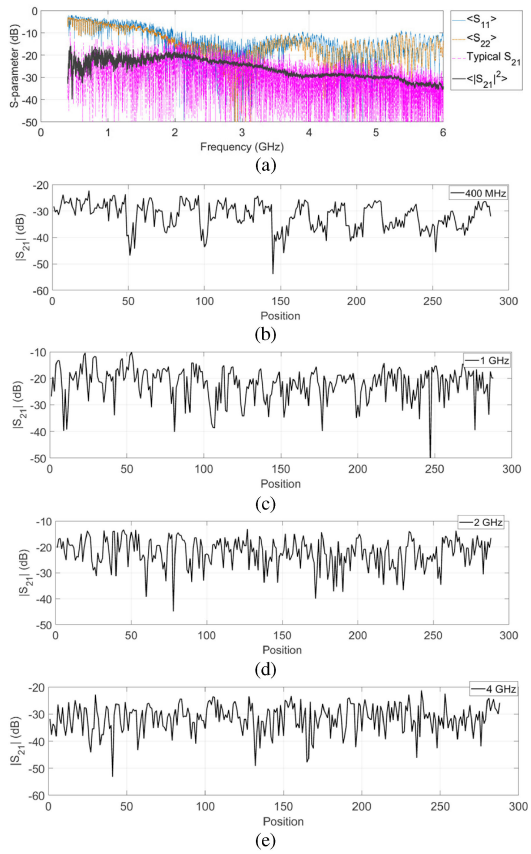

Fig. 3. Measured S-parameters. (a) S-parameters at different frequencies. (b)–(e) Measured S_{21} for different antenna positions (Ant 2).

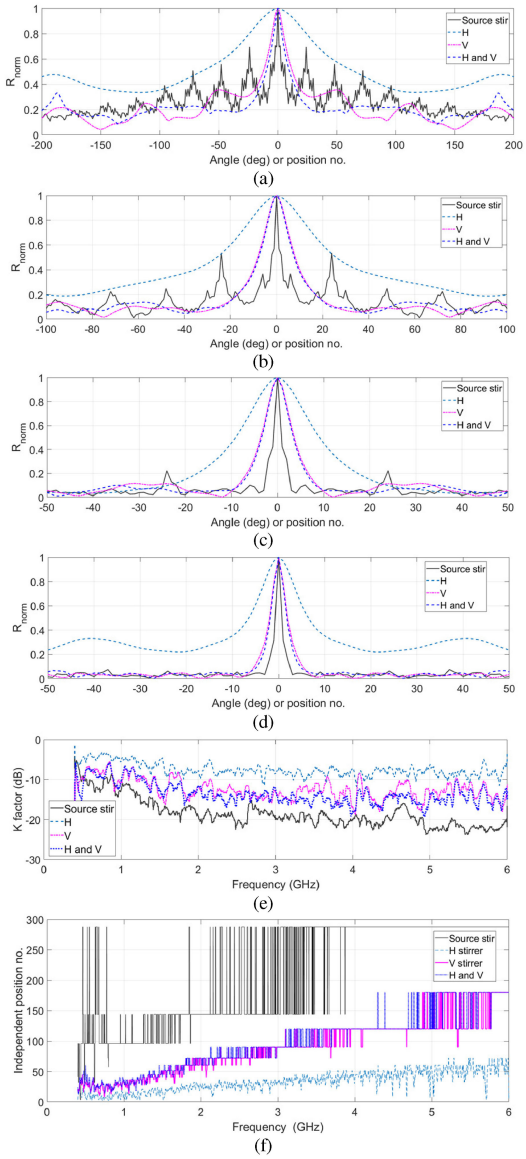

Fig. 4. Normalized autocorrelation for different frequencies: (a) 400 MHz, (b) 1 GHz, (c) 2 GHz, and (d) 4 GHz, (e) averaged K-factors ($\langle K \rangle_f$), (f) independent sample numbers; H and V means the H-stirrer and V-stirrer are rotated simultaneously.

In the measurement, considering the rotation angles of the 5 DoF, we use four samples for θ_1, three samples for θ_2, four samples for θ_3, three samples for θ_4, and two samples for θ_5, respectively. This makes $4 \times 3 \times 4 \times 3 \times 2 = 288$ positions in total. For each position of Ant 2, 56 001 samples of S-parameters are measured in the frequency range of 400 MHz to 6 GHz.

III. Measurement Results

The measured S-parameters are presented in Fig. 3 for different frequencies and antenna positions. Ant 1 and Ant 2 are the same type, thus $\langle S_{11} \rangle$ and $\langle S_{22} \rangle$ are very similar in Fig. 3(a). $\langle \cdot \rangle$ means the average over all stirrer/source positions. The measured S_{21} for different antenna positions are illustrated in Fig. 3(b)–(e). It can be observed that when the frequency is 400 MHz (much lower than the LUF), S_{21} is less sensitive to the source positions and shows a quasi-periodical behavior. When the frequency increases, significant randomness can be observed.

To characterize the performance of the source stir technique, we compare the figures of merit such as autocorrelation [1], [27]–[30], K-factor, [27], [31], [32] and total scattering cross-section (TSCS) [24], [33]–[36] for the source stir and the conventional mechanical stirrers. The setup for the conventional mechanical stirrers has been given in [26], where two stirrers were used: the horizontal stirrer (H) and the vertical stirrer (V). 360 stirrer positions with 1°/step were used for H or/and V stirrers. The normalized autocorrelations (R_{norm}) are shown in Fig. 4(a)–(d). The unit of the x-axis for the source stir autocorrelation is no longer degree but position no. As can be seen, at 400 MHz, the correlation is high for closed positions. When the frequency increases, the angular correlation of the source stir gives smaller correlations and outperforms H and/or V

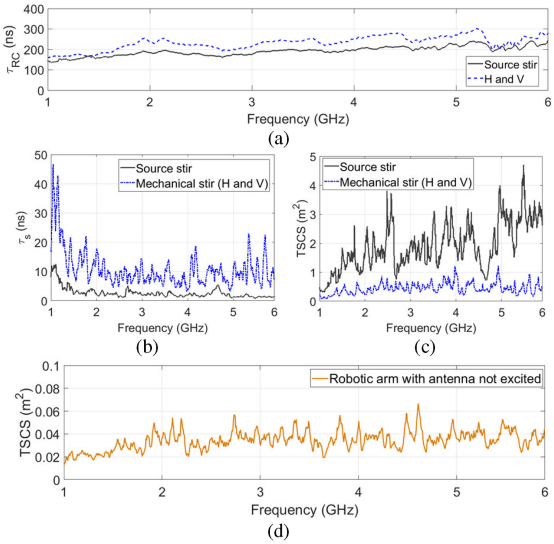

Fig. 5. (a) Measured chamber decay time. (b) Measured scattering damping time. (c) Measured equivalent TSCS. (d) Measured TSCS of the robotic arm when the source stir antenna is not excited.

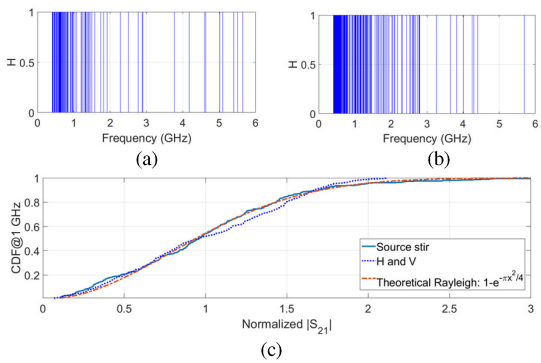

Fig. 6. Decision of the KS test: (a) source stir, (b) mechanical stir, both H- and V-stirrers are used, (c) CDFs of the normalized $|S_{21}|$ at 1 GHz, the CDF of the theoretical Rayleigh distribution is also plotted.

stirrers. This can also be observed from the *K*-factors averaged ove frequency ($\langle K \rangle_f$) in Fig. 4(e). Since the average autocorrelation and the *K*-factor are equivalent [26], Fig. 4(e) shows consistent results with Fig. 4(a)–(d) where the source stir scenario has the smallest average *K*-factor. The independent sample numbers [1] are also calculated and presented in Fig. 4(f), the stepped lines are caused by the finite angular resolution (or position no.) used in the measurements. As shown in Fig. 4(f), the source stir technique gives the highest values.

Besides the autocorrelation and *K*-factors, TSCS is a better quantity to quantify the stirring efficiency, because the loss in the RC can affect the *K*-factors [5] but not TSCS. The TSCS can be obtained from [27], we have

$$\tau_s = \langle K \rangle_f \tau_{\mathrm{RC}} / \left(1 - \langle K \rangle_f\right) \tag{1}$$

and

$$\mathrm{TSCS} = V / \left(c_0 \tau_s\right) \tag{2}$$

where τ_s is the scattering damping time, $\langle K \rangle_f$ is the averaged *K*-factor over the frequency, τ_{RC} is the chamber decay time, $c_0 = 3 \times 10^8$ m/s is the speed of light in free space, and V is the volume of the RC.

The chamber decay time (τ_{RC}) can be extracted by applying the inverse Fourier transform (IFT) of the measured *S*-parameters [25], [37]. The extracted values are given in Fig. 5(a) for the source stir and the mechanical stir scenarios. It is interesting to note that τ_{RC} for the source stir is slightly smaller than that for the mechanical stir. This could be due to the loss of the material (polylactic acid) [38], the driving motors and the printed circuit board of the motor controller. By applying (1) and (2), τ_s and the TSCS can be obtained and are illustrated in Fig. 5(b) and Fig. 5(c), respectively. Because the mechanical stirrer has a limit for the TSCS [33], but the source stir does not have (if the source can be moved freely in an RC). Not surprisingly, the source stir technique gives a higher equivalent TSCS and a higher stirring efficiency is achieved.

Since the robotic arm is moved, the mechanical structure can also stir the fields inside the RC. To identify the TSCS contributed by the mechanical structure of the robotic arm (including the antenna), we use the robotic arm (with the antenna loaded with 50 Ω) as a conventional mechanical stirrer and repeat the TSCS measurement. The measured TSCS is illustrated in Fig. 5(d), as can be seen, the values are very small and the source stirred TSCS is dominated by the source but not by the moving of the robotic arm.

To validate the statistical distribution of the frequency domain response, the cumulative distribution functions of the measured $|S_{21}|$ are checked by using the Kolmogorov–Smirnov (KS) test. A total of 288 samples at each frequency are used in the KS test; the results are given in Fig. 6 where $H = 0$ means the KS test fails to reject the hypothesis at 5% significance level, $H = 1$ means reject the hypothetical distribution. It can be found that the rejection rate of the source stir scenario (Fig. 6a) is lower than that of the mechanical stirrers (Fig. 6b). The statistical distribution of the measured $|S_{21}|$ is Rayleigh as expected for the frequencies above the LUF. The CDFs of the normalized $|S_{21}|$ (normalize to the mean value) at 1 GHz for the source stir and the mechanical stir scenarios are illustrated in Fig. 6(c), where the CDF from the source stir is closer to the theoretical curve than that from the mechanical stirrers.

IV. Conclusion

A 3-D printed robotic arm has been used to realize a source stirred RC which can generate a large amount of samples efficiently. The source stirring efficiency has been characterized by using the autocorrelation, the average *K*-factor, and the TSCS. The statistical distribution of the RC response has also been verified by using the KS test. Measurement results have shown that the source stir technique outperforms the conventional mechanical stir technique. In the meanwhile, the stirring volume (the volume occupied by the moving robotic arm and the antenna) for the source stir is 45 cm × 45 cm × 50 cm while the mechanical stirrers have stirring volumes of about 45 cm × 45 cm × 100 cm for the V-stirrer and 25 cm × 25 cm × 50 cm for the H-stirrer, respectively. It can be found that the source stir technique has a much smaller stirring volume. If the source stir antenna

is mounted on the roof of the RC, it could lead an RC with no stirrers, reduce the LUF, and increase the testing volume.

It is interesting to note that when calculating the autocorrelation for the source stirred RC, quasi-periodical high correlations are observed at low frequencies. This is because the antenna is moved to a closed position when a "for loop" for one angle variable is completed. Actually, the sequence of the results can affect the autocorrelation but not the average K-factor, the TSCS and the hypothesis test. Another thing to note is that when applying the source stir, the performance of the cable should not be sensitive to the position of the antenna. This may not be a problem for EMC applications, but if the antenna efficiency is of interest, the movement of the cable may introduce extra uncertainties at high frequencies.

REFERENCES

[1] *IEC 61000-4-21:2001,* Electromagnetic Compatibility (EMC)—Part 4-21: Testing and Measurement Techniques—Reverberation Chamber Test Methods, IEC Standard, Ed 2.0, Jan. 2011.

[2] D. A. Hill, *Electromagnetic Fields in Cavities: Deterministic and Statistical Theories*. Wiley-IEEE Press, USA, 2009.

[3] P. Besnier and B. Demoulin, *Electromagnetic Reverberation Chambers*. Wiley-ISTE, USA, 2011.

[4] P. S. Kildal, X. Chen, C. Orlenius, M. Franzen, and C. S. L. Patane, "Characterization of reverberation chambers for OTA measurements of wireless devices: Physical formulations of channel matrix and new uncertainty formula," *IEEE Trans. Antennas Propag.*, vol. 60, no. 8, pp. 3875–3891, Aug. 2012.

[5] C. L. Holloway, D. A. Hill, J. M. Ladbury, P. F. Wilson, G. Koepke, and J. Coder, "On the use of reverberation chambers to simulate a Rician radio environment for the testing of wireless devices," *IEEE Trans. Antennas Propag.*, vol. 54, no. 11, pp. 3167–3177, Nov. 2006.

[6] J. F. Valenzuela-Valdes, A. M. Martinez-Gonzalez, and D. A. Sanchez-Hernandez, "Diversity gain and MIMO capacity for nonisotropic environments using a reverberation chamber," *IEEE Antennas Wireless Propag. Lett.*, vol. 8, pp. 112–115, Jan. 2009.

[7] K. Rosengren and P.-S. Kildal, "Radiation efficiency correlation diversity gain and capacity of a six monopole antenna array for a MIMO system: Theory simulation and measurement in reverberation chamber," *Proc. Inst. Elect. Electron.—Microw. Antennas Propag.*, vol. 152, no. 1, pp. 7–16, Feb. 2005.

[8] F. Alhorr, M. Wiles, S. Fermiñán-Rodríguez, and C. Wehrmann, "On the comparison between anechoic and reverberation chambers for wireless OTA testing," in *Proc. 7th Eur. Conf. Antennas Propag.*, Gothenburg, 2013, pp. 1852–1856.

[9] A. Skårbratt, J. Åsberg, and C. Orlenius, "Over-the-air performance testing of wireless terminals by data throughput measurements in reverberation chamber," in *Proc. 5th Eur. Conf. Antennas Propag.*, Rome, 2011, pp. 615–619.

[10] Y. Huang, "*The investigation of chambers for electromagnetic systems*," *DPhil thesis*, Dept. of Engineering Science, Univ. Oxford, Oxford, U.K., 1993.

[11] Y. Huang and D. J. Edwards, "A novel reverberating chamber: Source-stirred chamber," in *Proc. IEEE 8th Int. Conf. Electromagn. Compat.*, Edinburgh, 1992, pp. 120–124.

[12] G. Cerri, V. M. Primiani, S. Pennesi, and P. Russo, "Source stirring mode for reverberation chambers," *IEEE Trans. Electromagn. Compat.*, vol. 47, no. 4, pp. 815–823, Nov. 2005.

[13] P. -S. Kildal and C. Carlsson, "Detection of a polarization imbalance in reverberation chambers and how to remove it by polarization stirring when measuring antenna efficiencies," *Microw. Opt. Technol. Lett.*, vol. 34, no. 2, pp. 145–149, 2002.

[14] E. Jackson and D. Zanette, "Stirred source and method of RFI testing," *Canada Patent CA2974054C*, Oct. 2, 2018.

[15] A. Cozza, "Source correlation in randomly excited complex media," *IEEE Antennas Wireless Propag. Lett.*, vol. 11, pp. 105–108, Jan. 2012.

[16] A. D. Leo, G. Cerri, P. Russo, and V. M. Primiani, "Experimental validation of an analytical model for the design of source-stirred chambers," *IEEE Trans. Electromagn. Compat.*, vol. 60, no. 2, pp. 540–543, Apr. 2018.

[17] A. De Leo, G. Cerri, P. Russo, and V. Mariani Primiani, "Experimental comparison between source stirring and mechanical stirring in a reverberation chamber by analyzing the antenna transmission coefficient," in *Proc. Int. Symp. Electromagn. Compat. (EMC EUROPE)*, Amsterdam, The Netherlands, 2018, pp. 677–682.

[18] G. Cerri, V. M. Primiani, C. Monteverde, and P. Russo, "A theoretical feasibility study of a source stirring reverberation chamber," *IEEE Trans. Electromagn. Compat.*, vol. 51, no. 1, pp. 3–11, Feb. 2009.

[19] V. M. Primiani, P. Russo, and G. Cerri, "Design and testing of an antenna system for the source stirring technique in reverberation chambers," *J. Electromagn. Waves Appl.*, vol. 26, pp. 837–850, 2012.

[20] A. De Leo, V. M. Primiani, P. Russo, and G. Cerri, "Numerical analysis of a reverberation chamber: Comparison between mechanical and source stirring techniques," in *Proc. Int. Symp. Electromagn. Compat. (EMC EUROPE)*, Angers, 2017, pp. 1–6.

[21] A. De Leo, V. M. Primiani, P. Russo, and G. Cerri, "Low-frequency theoretical analysis of a source-stirred reverberation chamber," *IEEE Trans. Electromagn. Compat.*, vol. 59, no. 2, pp. 315–324, Apr. 2017.

[22] A. De Leo, V. M. Primiani, P. Russo, and G. Cerri, "Optimization techniques for source stirred reverberation chambers," in *Proc. Int. Symp. Electromagn. Compat. (EMC EUROPE)*, Wroclaw, 2016, pp. 199–204.

[23] A. Cozza, W. J. Koh, Y. S. Ng, and Y. Y. Tan, "Controlling the state of a reverberation chamber by means of a random multiple-antenna stirring," in *Proc. Asia-Pacific Symp. Electromagn. Compat.*, Singapore, 2012, pp. 765–768.

[24] Q. Xu, Y. Huang, L. Xing, Z. Tian, M. Stanley, and S. Yuan, "B-Scan in a reverberation chamber," *IEEE Trans. Antennas Propag.*, vol. 64, no. 5, pp. 1740–1750, May 2016.

[25] Q. Xu and Y. Huang, *Anechoic and Reverberation Chambers: Theory, Design and Measurements*. Wiley-IEEE, U.K., 2019.

[26] Q. Xu, L. Xing, Y. Zhao, T. Loh, M. Wang, and Y. Huang, "Approximate analytical equations for the stirrer angular correlation in a reverberation chamber," *IEEE Trans. Electromagn. Compat.*, pp. 1–7, Nov. 2018, doi: 10.1109/TEMC.2018.2879431.

[27] Q. Xu, L. Xing, Y. Zhao, Z. Tian, and Y. Huang, "Wiener–Khinchin theorem in a reverberation chamber," *IEEE Trans. Electromagn. Compat.*, 2018, doi: 10.1109/TEMC.2018.2863297.

[28] Q. Xu, L. Xing, D. Yan, Y. Zhao, T. Jia, and Y. Huang, "Experimental verification of stirrer angular correlation with different definitions in a reverberation chamber," in *Proc. 12th Int. Symp. Antennas, Propag. EM Theory*, Hangzhou, China, 2018, pp. 1–4.

[29] K. Karlsson, X. Chen, P.-S. Kildal, and J. Carlsson, "Doppler spread in reverberation chamber predicted from measurements during step-wise stationary stirring," *IEEE Antennas Wireless Propag. Lett.*, vol. 9, pp. 497–500, May 2010.

[30] X. Chen, P.-S. Kildal, and J. Carlsson, "Determination of maximum doppler shift in reverberation chamber using level crossing rate," in *Proc. 5th Eur. Conf. Antennas Propag.*, Rome, Italy, 2011, pp. 62–65.

[31] C. Lemoine, E. Amador, and P. Besnier, "Mode-stirring efficiency of reverberation chambers based on Rician K-factor," *Electron. Lett.*, vol. 47, no. 20, pp. 1114–1115, Sep. 2011.

[32] X. Chen, P.-S. Kildal, and S.-H. Lai, "Estimation of average rician K-factor and average mode bandwidth in loaded reverberation chamber," *IEEE Antennas Wireless Propag. Lett.*, vol. 10, pp. 1437–1440, Dec. 2011.

[33] Q. Xu, Y. Huang, L. Xing, Z. Tian, C. Song, and M. Stanley, "The limit of the total scattering cross section of electrically large stirrers in a reverberation chamber," *IEEE Trans. Electromagn. Compat.*, vol. 58, no. 2, pp. 623–626, Apr. 2016.

[34] G. Lerosey and J. de Rosny, "Scattering cross section measurement in reverberation chamber," *IEEE Trans. Electromagn. Compat.*, vol. 49, no. 2, pp. 280–284, May 2007.

[35] S. Lallechere, I. E. Baba, P. Bonnet, and F. Paladian, "Total scattering cross section improvements from electromagnetic reverberation chambers modeling and stochastic formalism," in *Proc. 5th Eur. Conf. Antennas Propag.*, Rome, Italy, 2011, pp. 81–85.

[36] I. E. Baba, S. Lallechere, P. Bonnet, J. Benoit, and F. Paladian, "Computing total scattering cross section from 3-D reverberation chambers time modeling," in *Proc. Asia-Pac. Symp. Electromagn. Compat.*, Singapore, 2012, pp. 585–588.

[37] Q. Xu, Y. Huang, L. Xing, and Z. Tian, "Extract the decay constant of a reverberation chamber without satisfying Nyquist criterion," *IEEE Microw. Wireless Compon. Lett.*, vol. 26, no. 3, pp. 153–155, Mar. 2016.

[38] T. Nakagawa, T. Nakiri, R. Hosoya, and Y. Tajitsu, "Electrical properties of biodegradable polylactic acid film," *IEEE Trans. Industry Appl.*, vol. 40, no. 4, pp. 1020–1024, Jul./Aug. 2004.